Available online at www.sciencedirect.com
SCIENCE DIRECT®
Journal of Sound and Vibration 283 (2005) 1137–1155
JOURNAL OF SOUND AND VIBRATION
www.elsevier.com/locate/jsvi

A time and frequency domain approach for identifying nonlinear mechanical system models in the absence of an input measurement

Muhammad Haroon[a], Douglas E. Adams[a,*], Yiu Wah Luk[b], Aldo A. Ferri[c]

[a]*School of Mechanical Engineering, Purdue University, Ray W. Herrick Laboratories, 140 S. Intramural Drive, West Lafayette, IN 47907-2031, USA*
[b]*Goodyear Tire & Rubber Company, Goodyear Vehicle Systems Technical Center D/480C, P.O. Box 3531, Akron, OH 44309-3531, USA*
[c]*Georgia Institute of Technology, The George W. Woodruff School of Mechanical Engineering, Atlanta, GA 30332-0405, USA*

Received 9 October 2003; accepted 3 June 2004
Available online 15 December 2004

Abstract

Conventional system identification procedures require that input data or at least an estimate of the input be used in the parameter estimation process. In many 'real' mechanical systems inputs are not readily measured, as in automotive road vehicle data in which the input to the tire patch of the tires from the road is neither measurable nor easy to estimate. A new method for nonlinear system identification of mechanical systems, in the absence of an input measurement, using a combination of time and frequency domain techniques is presented here. In the time domain, restoring force plots are used to characterize the frequency and amplitude characteristics of the nonlinearities. These observed nonlinear characteristics are then used in the output-only formulation of the nonlinear identification through feedback of the outputs frequency domain parameter estimation technique to build a model with linear and nonlinear frequency response functions, which can be used to predict the response of the system. The method is applied to experimental tire-vehicle suspension system data.

*Corresponding author. Tel.: +1-765-496-6033; fax: +1-765-494-0787.
E-mail addresses: mharoon@purdue.edu (M. Haroon), deadams@ecn.purdue.edu (D.E. Adams), yw_luk@goodyear.com (Y.W. Luk), al.ferri@me.gatech.edu (A.A. Ferri).
URL: http://widget.ecn.purdue.edu/~FEND2.

0022-460X/$ - see front matter © 2004 Elsevier Ltd. All rights reserved.
doi:10.1016/j.jsv.2004.06.008

1. Introduction

Much work has been done in the area of nonlinear system identification for mechanical systems. Mohammad et al. [1] introduced the direct parameter estimation method, which uses recursive least squares to estimate the parameters of a linear or nonlinear multidegree-of-freedom system given just one input. Richards and Singh [2] presented a "reverse path" spectral method, which was derived from Bendat's [3] earlier work for single input nonlinear systems, for the identification of multidegree-of-freedom nonlinear systems for Gaussian random inputs. Roberts et al. [4] presented a spectral method for estimating nonlinear parameters in cases when it is either impractical or impossible to measure the excitation process. The unmeasured excitation was modeled as a stationary stochastic process with zero mean.

Masri et al. [5,6] presented a time domain method that uses recursive least squares along with modal analysis for linear parameter identification and a non-parametric method for expressing the nonlinear characteristics in terms of orthogonal functions. Yi and Hedrick [7] studied a technique for identifying nonlinear system parameters based on a least-squares method and a "sliding observer" that allows the estimation of signals that are difficult or expensive to measure. Adams and Allemang [8] introduced the frequency domain nonlinear identification through feedback of the outputs (NIFO) method, which decouples the linear and nonlinear dynamics of a system and estimates the linear and nonlinear components in one computational step. This approach is expanded upon in the present paper to permit the use of response data in the absence of input measurements.

Most of the prior research recognizes that proper characterization of the nonlinearities in a system is necessary for applying system identification processes. Popular characterization techniques include frequency deconvolution [9], Hilbert transforms [10,11], and wavelet transforms [12]. In addition, Storer and Tomlinson [13] used higher-order frequency response functions to characterize nonlinear structural dynamic systems. Cafferty et al. [14] used the restoring force method to characterize the dynamic properties of automotive dampers and Audenino and Belingardi [15] also recognized the merit of this method.

This literature survey presents a small but representative portion of the research in the area of nonlinear system characterization and identification for mechanical systems. All of these prior system identification methods require an input measurement or at least an estimate of the input. Identification and even characterization in the absence of an input measurement has not been studied in detail. In many types of mechanical systems, like tire-vehicle suspension systems, the input measurement is not readily measurable when taking operating data.

In this paper, a system identification approach is presented that uses both time and frequency domain techniques to develop a model of a system with both linear and nonlinear functions in the absence of an input measurement. In this approach, the restoring force method is used to characterize the frequency and amplitude characteristics of the nonlinearities observed in the system. The attractive aspect of the restoring force method is that it only requires the output acceleration measurements of the degrees-of-freedom between which the nonlinearities are to be characterized. The NIFO frequency domain method is then formulated in terms of the responses

of the system. The characteristics of the nonlinearities observed in restoring force plots are used in NIFO to identify the operating point response of the system in addition to the nonlinear contributions. This approach provides a frequency domain model that describes how the system responses change with changes in both input amplitude and frequency.

The next section establishes a framework for the proposed approach. The approach is then applied to experimental vehicle data to demonstrate its validity. The time domain characterization procedure (restoring force method) is described first followed by the frequency domain identification procedure (NIFO).

2. Framework

2.1. Restoring force

The restoring force is an internal force that opposes the motion of an inertial element within a system, e.g., the left-hand side of Newton's Second Law for a body with constant mass, m, and acceleration vector, $\mathbf{a}$: $\Sigma\mathbf{F} = m\mathbf{a}$. The stiffness and damping in a system resist the motion of a given inertia; consequently, the forces in the stiffness and damping elements are referred to as components of the restoring forces. Individual nonlinearities have particular restoring forces; therefore, nonlinearities can be characterized by the restoring forces within a system.

Broadly speaking, restoring forces can be "static" or "dynamic" in nature. Static nonlinearities produce restoring forces that depend only on the instantaneous relative displacement or relative velocity between two connection points. Several common examples of static nonlinearities associated with particular stiffness and damping characteristics are shown in Fig. 1. Dynamic nonlinearities, which are usually characterized by differential operators, give rise to restoring forces that depend not only on the present displacement and velocity, but also on the history of the motion. An example of such a nonlinearity is a nonlinear hysteretic stiffness. The present paper considers only static nonlinearities.

As mentioned previously, the chief advantage of the restoring force technique is that it only requires that the output accelerations of a system be measured. Consider the two degree-of-freedom quarter car model shown in Fig. 2. The equations of motion for this system are given by

$$\begin{aligned} &M_1\ddot{x}_1 + (C_1 + C_2)\dot{x}_1 - C_2\dot{x}_2 + (K_1 + K_2)x_1 - K_2x_2 + N_1[x_1(t), x_2(t), \dot{x}_1(t)\dot{x}_2(t)] \\ &\quad + N_2[x_1(t), x_b(t), \dot{x}_1(t)\dot{x}_b(t)] = C_1\dot{x}_b + K_1x_b \\ &M_2\ddot{x}_2 - C_2\dot{x}_1 + C_2\dot{x}_2 - K_2x_1 + (K_2 + K_3)x_2 = N_1[x_1(t), x_2(t), \dot{x}_1(t)\dot{x}_2(t)], \end{aligned} \tag{1}$$

where $x_k(t)$ are the displacements of the unsprung and sprung masses, M_k, $x_b(t)$ is the displacement of the tire patch, C_k and K_k are the damping and stiffness in the tire and suspension, $N_1[x_1(t), x_2(t), \dot{x}_1(t)\dot{x}_2(t)]$ denotes the nonlinear forces in the suspension and $N_2[x_1(t), x_b(t), \dot{x}_1(t)\dot{x}_b(t)]$ denotes the nonlinear forces in the tire.

The second equation, for the sprung mass, M_2, can be rearranged to give the following expression for the restoring force in the suspension:

$$M_2\ddot{x}_2 = -C_2(\dot{x}_2 - \dot{x}_1) - K_2(x_2 - x_1) - K_3x_2 + N_1[x_1(t), x_2(t), \dot{x}_1(t), \dot{x}_2(t)]. \tag{2}$$

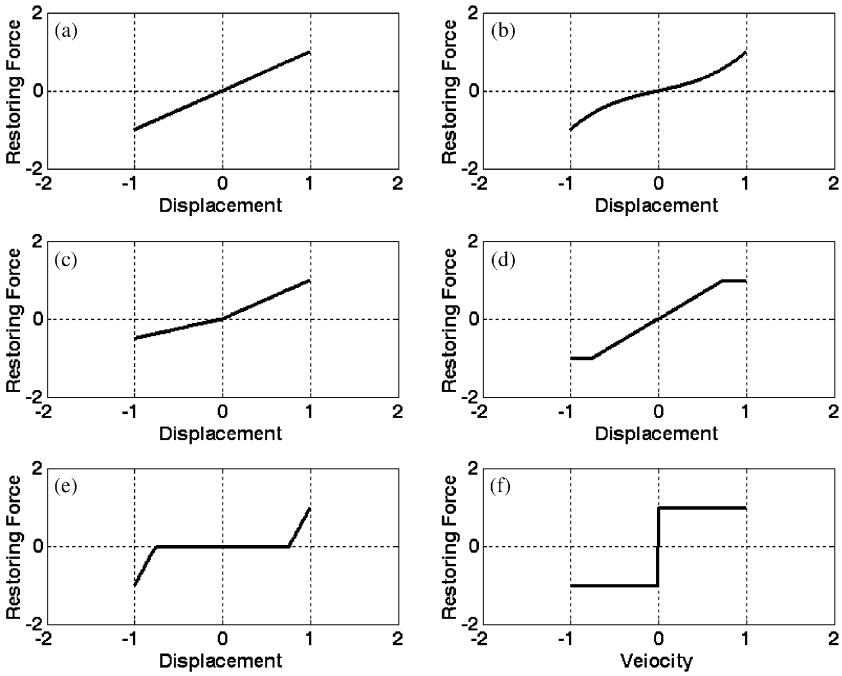

Fig. 1. Idealized forms of simple structural, (b) cubic hardening stiffness, (c) piecewise-linear stiffness, (d) saturation force, (e) clearance force and (f) Coulomb friction damping compared to a linear stiffness restoring force (a).

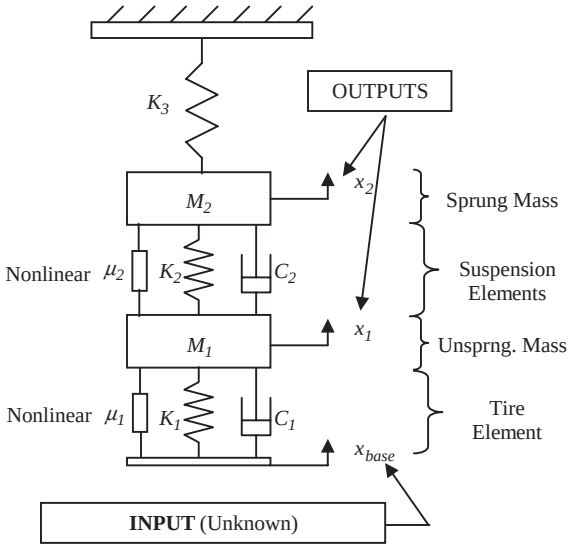

Fig. 2. Quarter car model.

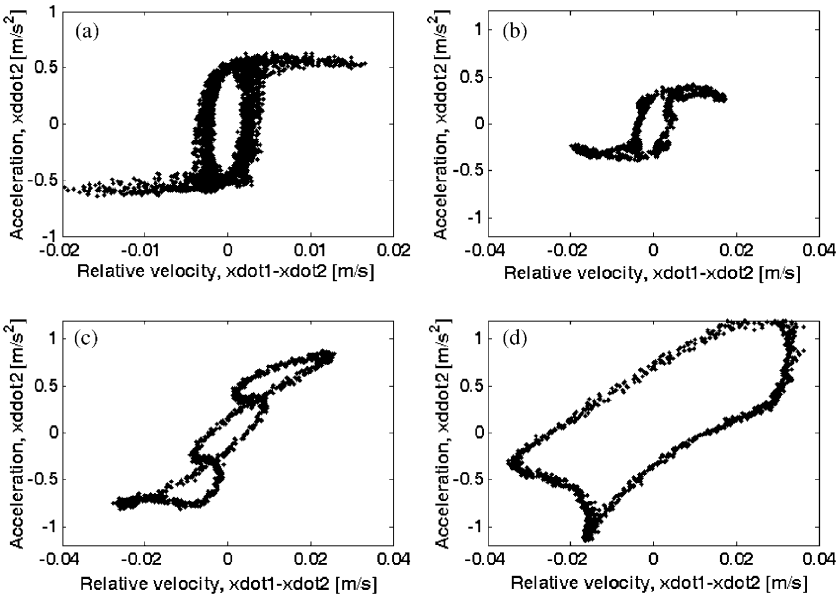

Fig. 3. Velocity restoring force in suspension system showing change in nonlinear damping with frequency for constant input amplitude at 0.5 mm stroke at the tire patch: (a) 3.8 Hz base excitation; (b) 5 Hz; (c) 8.4 Hz; and (d) 14.2 Hz.

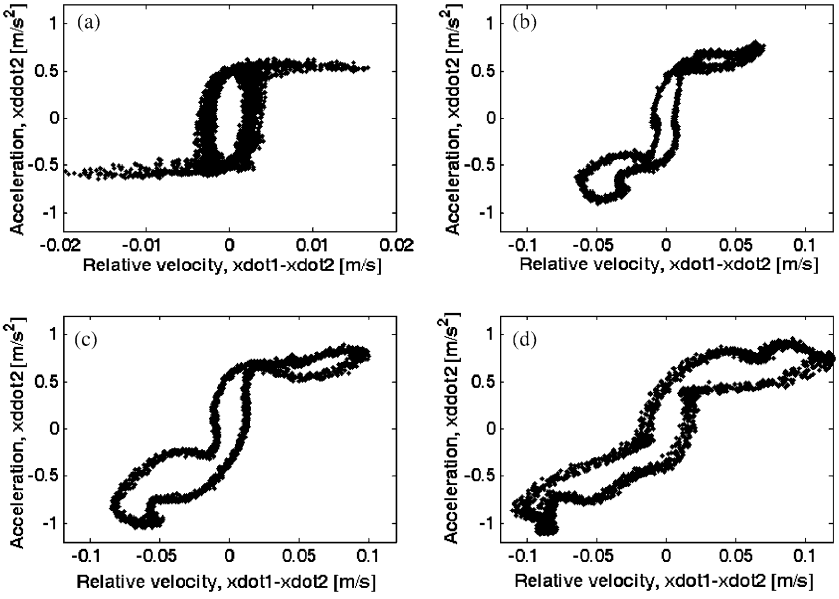

Fig. 4. Velocity restoring force in suspension system showing change in nonlinear damping with amplitude for constant frequency input at 3.8 Hz at the tire patch: (a) 0.5 mm base excitation; (b) 2.0 mm; (c) 3.0 mm; and (d) 4.0 mm.

The plot between the acceleration of the sprung mass and the relative velocity between the sprung mass and the unsprung mass allows the damping restoring force in the suspension to be characterized. Similarly, the plot between the acceleration of the sprung mass and the relative

displacement between the sprung mass and the unsprung mass allows the stiffness restoring force in the suspension to be characterized. Figs. 3 and 4 show the damping restoring force plots for different input frequencies (3.8–14.2 Hz for Fig. 3(a)–(d)) at constant amplitude (0.5 mm) and different amplitudes (0.5–4.0 mm for Fig. 4(a)–(d)) at constant frequency (3.8 Hz). Note that both frequency and amplitude dependence of the nonlinearities are observed in the suspension system of an experimental vehicle, thereby requiring that a frequency domain system identification method be employed to properly characterize nonlinear changes with amplitude and linear changes with frequency.

This example demonstrates that only response measurements for the sprung mass and the unsprung mass are needed to characterize certain nonlinearities in the suspension system. Furthermore, in experimental system identification, acceleration measurements are the most convenient measurements to make and can also be integrated to estimate velocity and displacement time histories so restoring force methods are especially appropriate for experimental purposes. Note, however, that the static (DC) components of the velocity and displacement time histories are lost in the integration process; consequently, certain types of nonlinearities such as quadratic stiffness nonlinearities, which produce steady streaming (i.e., a DC response), may be difficult to identify.

2.2. Nonlinear identification through feedback of the outputs (NIFO)

The nonlinearities present in a system create unmeasured, correlated internal feedback forces in the linear model of the system. In other words, in nonlinear systems, the external inputs act together with the internal nonlinear feedback forces on the underlying linear system to produce the measured outputs of the system. This combination of external and internal forces is evident in the following impedance model formulation for an arbitrary lumped parameter mechanical system,

$$[B_L(\omega)]\{X(\omega)\} = \{F(\omega)\} - \sum_{i=1}^{N} \mu_i(\omega)\{B_{ni}\}X_{ni}(\omega), \tag{3}$$

$$= \{F(\omega)\} + \{F_n(\omega)\}, \tag{4}$$

where $[B_L(\omega)]$ is the linear impedance matrix, $\mu_i(\omega)$ are the nonlinear (frequency dependent) coefficients, $X_{ni}(\omega)$ are scalar Fourier transforms of the nonlinear restoring forces of the outputs, which account for the internal feedback forces, and N is the number of nonlinearities included in the model. Each non-zero element of incidence vector, $\{B_{ni}\}$, is either a 1 or a -1; these elements determine the location of the nonlinearity. A different $\{B_{ni}\}$ and $X_{ni}(\omega)$ pair is used to model each nonlinear element in the system. Fig. 5 illustrates the concept of internal feedback by the nonlinearities and superposition of the external forces and the internal feedback forces.

The NIFO parameter estimation formulation is derived from Eq. (3) by multiplying both sides of the equation on the left by the linear system (square) FRF matrix, $[H_L(\omega)]$, and separating the

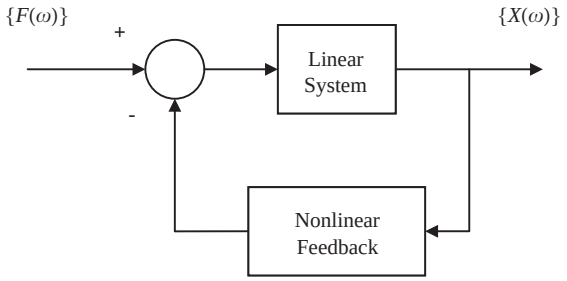

Fig. 5. Feedback by nonlinearities into a linear vibrating system illustrating the superposition of the external forces and the internal feedback forces.

measured and unmeasured quantities as follows:

$$\{X(\omega)\} = [[H_L(\omega)][H_L(\omega)]\mu_1(\omega)\{B_{n1}(\omega)\}[H_L(\omega)]\mu_2(\omega)\{B_{n2}(\omega)\} \times [H_L(\omega)]\mu_N(\omega)\{B_{nN}(\omega)\}] \left(\begin{Bmatrix} \{F(\omega)\} \\ 0 \end{Bmatrix} - \begin{Bmatrix} X_{n1}(\omega) \\ X_{n2}(\omega) \\ \vdots \\ X_{nN} \end{Bmatrix} \right). \quad (5)$$

If the inputs and the outputs can be measured, and because the nonlinear functions can be calculated explicitly in terms of the measured inputs and the outputs, the set of equations in Eq. (5) can be used to estimate the best unbiased least-squares estimate of the linear FRFs at the forced DOFs and the nonlinear parameters $\mu_i(\omega)$ at forced and unforced DOFs in a single step. It is important to note that although most system identification procedures tend to associate the nominal linear FRFs in $[H_L(\omega)]$ with the lowest level measured input and output data, many nonlinear mechanical systems contain nonlinearites that are most severe for the lowest level excitations. Moreover, nonlinearites like Coulomb friction damping forces, which are not continuous, do not significantly affect the dynamics for large relative motions, indicating that the nominal linear FRFs in $[H_L(\omega)]$ are actually associated with high-level input and output data. More will be said about this issue in the context of the experimental results in Section 3.

When the input cannot be measured, the formulation for NIFO must be modified. This modification is best explained in the context of an example. Consider the two DOF quarter car model illustrated in Fig. 2. The equation of motion for the sprung mass (ignoring damping) can be written in the frequency domain for zero initial conditions as follows when the nonlinear elements in Fig. 2 are taken to be frequency independent,

$$(-\omega^2 M_2 + K_2 + K_3)X_2(\omega) = K_2 X_1(\omega) + \mu_1 X_{n1}(\omega) + \mu_2 X_{n2}(\omega). \quad (6)$$

In this equation, $X_{n1}(\omega)$ and $X_{n2}(\omega)$ are the Fourier transforms of two particular suspension nonlinear restoring forces of interest, called 'describing functions', and μ_1 and μ_2 are the

corresponding nonlinear coefficients, assumed constant here, that determine the nonlinear weightings. This equation can be rewritten in the following form to highlight the presence of the nominal linear transmissibility function:

$$X_2(\omega) = \frac{K_2}{-\omega^2 M_2 + K_2 + K_3} X_1(\omega) + \frac{\mu_1}{-\omega^2 M_2 + K_2 + K_3} X_{n1}(\omega) + \frac{\mu_2}{-\omega^2 M_2 + K_2 + K_3} X_{n2}(\omega). \tag{7}$$

Note that the coefficient of $X_1(\omega)$, $K_2/(-\omega^2 M_2 + K_2 + K_3)$, is equal to the transmissibility between the body and wheel displacements of the underlying linear two DOF system (i.e., ratio of $X_2(\omega)$ to $X_1(\omega)$ when μ_1 and μ_2 are both identically zero); consequently, the nonlinear terms in the second and third expressions on the right hand side of this equation determine the extent to which the system vibrates away from the operating point due to the presence of the nonlinearities.

If the linear transmissibility function is replaced with the notation $T_{21}(\omega)$, Eq. (7) can be written in matrix form as

$$X_2(\omega) = \begin{bmatrix} T_{21}(\omega) & \frac{\mu_1}{K_2} T_{21}(\omega) & \frac{\mu_2}{K_2} T_{21}(\omega) \end{bmatrix} \begin{bmatrix} X_1(\omega) \\ X_{n1}(\omega) \\ X_{n2}(\omega) \end{bmatrix}. \tag{8}$$

Eq. (8) relates the wheel response at the spindle, which acts as an input to the vehicle body in addition to the two nonlinear restoring forces, to the body response and is equivalent to a three input, single output frequency domain model. Because the three inputs are not completely correlated at any given frequency, a least-squares parameter estimation procedure can be carried out to calculate the three coefficient functions in the row matrix on the right-hand side of the equation using spectral averaging via cross- and auto-power spectra. For example, if repeated runs using broadband stochastic (random) excitation are carried out, the results from each can be assembled as shown in Eq. (9):

$$\{ X_2(\omega)_1 \quad X_2(\omega)_2 \quad . \quad X_2(\omega)_{N_{\text{avg}}} \}_{1\times N_{\text{avg}}} = \begin{bmatrix} T_{21}(\omega) & \frac{\mu_1}{K_2} T_{21}(\omega) & \frac{\mu_2}{K_2} T_{21}(\omega) \end{bmatrix}_{1\times 3} \times \begin{bmatrix} X_1(\omega)_1 & X_1(\omega)_2 & . & . & X_1(\omega)_{N_{\text{avg}}} \\ X_{n1}(\omega)_1 & X_{n1}(\omega)_2 & . & . & X_{n1}(\omega)_{N_{\text{avg}}} \\ X_{n2}(\omega)_1 & X_{n2}(\omega)_2 & . & . & X_{n2}(\omega)_{N_{\text{avg}}} \end{bmatrix}_{3\times N_{\text{avg}}}, \tag{9}$$

where N_{avg} is the number of spectral averages. In order to solve this equation for the given number of spectral averages, the Hermitian transpose of the matrix on the right-hand side is multiplied on the right of both sides of the equation, thus producing cross- and auto-power matrices with the body response data matrix and itself. These matrices are then amenable to standard cumulative spectral processing operations via H_1 or H_2 calculations, whichever is more appropriate for the given assumptions regarding measurement noise. In this work, it is assumed that the measurements are relatively noise free but that the small amount of noise that is present contaminates the X_2 (body side) data only. Note that unlike linear system identification, even uncorrelated response measurement noise can seriously corrupt the parameter estimates for

nonlinear systems because the nonlinear describing functions (i.e., $X_{n1}(\omega)$ and $X_{n2}(\omega)$) always result in correlated noise.

It is evident from the formulation in Eq. (9) that nonlinearities must first be characterized prior to applying the system identification procedure because the describing functions are needed to form the matrix on the far right-hand side of Eq. (9). Hence, nonlinear characterization via the time domain restoring force technique described earlier is a very important first step in the following system identification procedure.

3. Experimental verification

The system identification procedure presented in the previous section is applied to laboratory vehicle data in this section.

3.1. Experimental setup

Response data were taken on the front left tire of an Isuzu Impulse using a hydraulic shaker apparatus. The fact that the vehicle had an independent front suspension meant that the results from the left and right front tires were the same and so only data from the front left tire were used. A picture of the experimental setup is shown in Fig. 6. The MTS® hydraulic shaker, with a maximum dynamic pressure of 3000 psi, an input frequency range of 0–100 Hz and a maximum stroke of approximately 8 in, was used to excite the tire patch of the car with different types of

Fig. 6. Shaker testing setup with single corner of vehicle shown.

inputs in the vertical direction. Although small motions were also observed in the lateral and longitudinal directions, only vertical motions will be considered here because they were dominant in the tests. Tri-axial accelerometers of nominal sensitivity 1 V/g were attached at the upper strut connection with the body $\ddot{x}_2(t)$, representing the sprung mass and the spindle $\ddot{x}_1(t)$, representing the unsprung mass, to measure the accelerations of these two DOFs. The displacement of the wheel pan (i.e., tire patch) was measured directly using the LVDT internal to the hydraulic actuator.

The signals were recorded with an IOTECH® Portable Data Acquisition System and converted into '.mat' files for further analysis in MATLAB®. The IOTECH® system allowed a wide range of sampling frequencies and the application of high- and/or low-pass filters to remove noise and aliasing from higher-frequency components.

3.2. Nonlinear characterization

As described earlier, the first step in system identification is the characterization of the observed nonlinearities in the system. A very slow chirp input to avoid abnormal transitions through nonlinear resonances (i.e., lingering bifurcations or other effects) from 0 to 15 Hz, at a rate of 0.025 Hz/s, was used as the base excitation for this purpose. The acceleration response measurements were taken and then integrated off-line to estimate the velocity and displacement responses. The signal processing parameters that were used are given in Table 1. A 50 Hz bandwidth low-pass filter was used to reduce aliasing back into the frequency range of interest from approximately 3–35 Hz.

Velocity (damping) and displacement (stiffness) restoring force curves were generated for different input amplitudes and frequencies. Fig. 7 shows two representative restoring force curves for an input amplitude of 0.5 mm and an input frequency of 3.8 Hz. The first curve, Fig. 7(a), is a function of the velocity and the second curve, Fig. 7(b), is a function of the displacement. The velocity curve (Fig. 7(a)) shows a nonlinear damping characteristic with both saturation (Coulomb friction damping curve) and hysteresis. The displacement curve 7(b) shows a nonlinear stiffness characteristic with primarily hysteresis (i.e., backlash). These two types of nonlinearities are present to various degrees across the entire frequency range. At this point in the characterization procedure, it is not clear whether or not hysteresis is present in the strut damping characteristic, strut stiffness characteristic or both. Note that the only nonlinearities present in Fig. 7 (and Figs. 3 and 4) are within the strut because no tire nonlinearities contribute to the forces on the body or the curves in these plots.

Recall that Fig. 3, which was mentioned earlier, shows the change in nonlinear strut damping force with frequency at a constant 0.5 mm input amplitude. The trends in the curves of

Table 1
Signal processing parameters for the chirp input

Chirp range (Hz)	Chirp rate (Hz/s)	Number of time points, N_t	Sampling frequency, F_s (Hz)	Low-pass filter (LPF) cut-off (Hz)
0–15	0.025	180,000	300	50

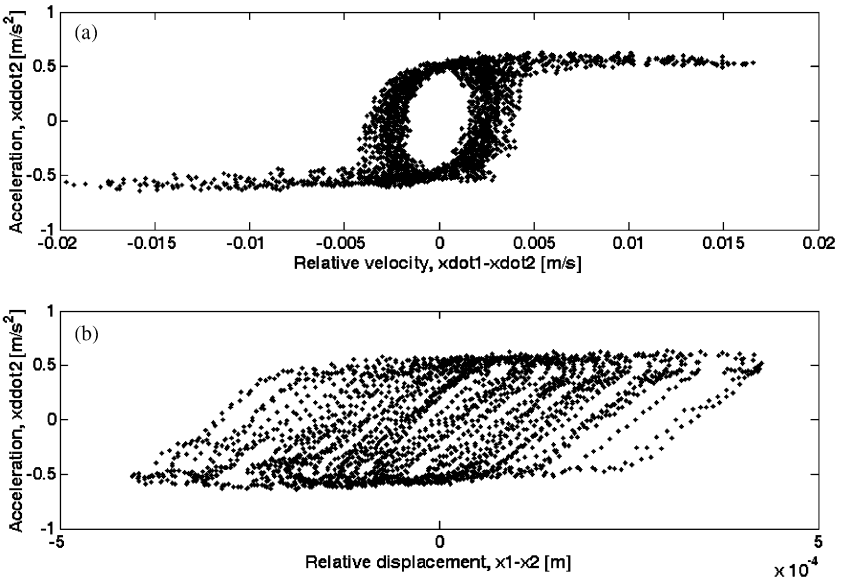

Fig. 7. (a) Nonlinear shock damping showing saturation at a certain relative clearance velocity and (b) nonlinear hysteretic stiffness showing backlash characteristic in both damping and stiffness; input amplitude 0.5 mm and input frequency 3.8 Hz.

Figs. 3(a)–(d) indicate that some of the nonlinear effects decrease as the frequency increases. This trend occurs because an increase in frequency results in an increase in stroke velocity and, hence, a gradual movement of the system away from the central hysteresis loop in Fig. 3(a) to the outer relatively linear portion of the restoring force curve in Fig. 3(d). It is anticipated that this linearization of the system damping force at higher frequencies will be reflected in the system identification results.

Fig. 4 shows the change in nonlinear damping force with amplitude at a constant frequency of 3.8 Hz. The damping characteristic changes from a saturation type in Fig. 4(a) to a piecewise-linear form in Fig. 4(d), in which positive relative velocities suffer more saturation than negative velocities, as anticipated in a typical shock absorber. This type of asymmetric nonlinearity is desirable to improve handling when traversing negative obstacles (i.e., potholes) without disturbing ride when traversing positive obstacles (i.e., speed bumps). The multiple loops in the restoring force curves, as shown in Fig. 3(c), are due to the presence of harmonics of the fundamental frequency in the data, which we recall was taken for a slowly varying chirp displacement input at the base of the tire.

Having characterized the properties of the nonlinearities, these nonlinear describing functions can now be used in a frequency domain parameter estimation algorithm such as NIFO for nonlinear system identification.

3.3. Nonlinear system identification

NIFO was applied to random input data with a Gaussian distribution for various input amplitudes ranging from 0.5 to 7.0 mm RMS displacements of the wheel pan (i.e., tire patch). The

Table 2
Signal processing parameters for spectral averaging with random input

Time points, N_t	Sampling frequency, F_s (Hz)	Block size, BS	Number of averages, N_{avg}	Overlap	Window type	LPF cut-off (Hz)	FRF estimator
180,000	600	6144	60	52%	Flattop	200	H_1

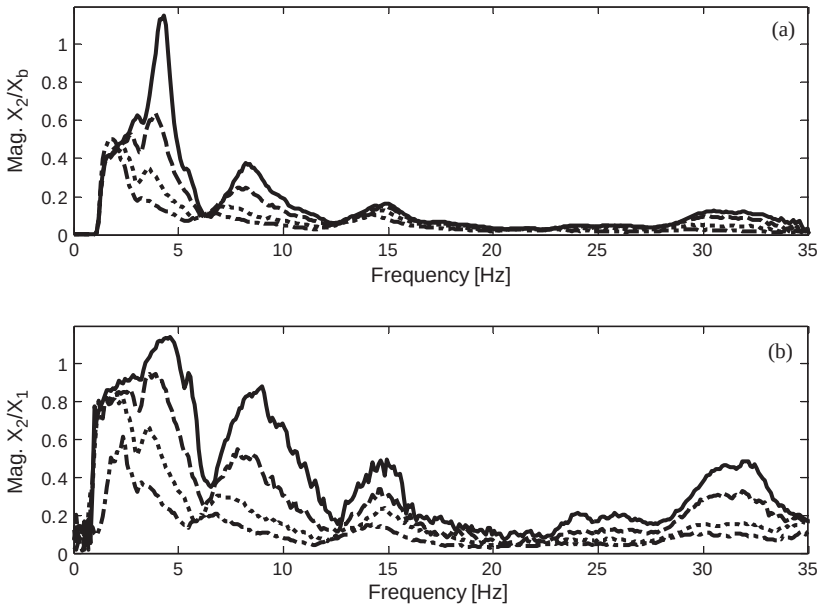

Fig. 8. Magnitudes of measured transmissibility functions between: (a) the tire patch and body side of the strut and (b) the spindle and the body for four different levels of excitation: —, 0.5 mm; – – –, 1.0 mm; ⋯, 2.5 mm; and – · –, 7.0 mm.

signal processing parameters used in these post-processing operations are given in Table 2. In this section, nonlinear identification is first used to develop linear and nonlinear models between the spindle and body using response data only (transmissibility). Then the input data at the tire patch is used to show that the effects of the tire are negligible in this operating range.

Fig. 8(a) shows the transmissibility functions between the sprung mass (x_2) and the tire patch (x_b) and Fig. 8(b) shows the transmissibility functions between the sprung mass (x_2) and the unsprung mass (x_1) for four different excitation amplitudes: (—) 0.5 mm, (– – –) 1.0 mm, (⋯) 2.5 mm and (– · –) 7.0 mm. Input amplitudes less than 0.5 mm produced noisy data and are not used in this analysis. There are clear changes in the transmissibility magnitudes, with and without using the input measurement, (x_b), indicating the presence of nonlinearity in the strut and possibly the tire as well (Fig. 8(a)). It should be noted that tire nonlinearities do not influence the transmissibility plot between the sprung mass and the unpsrung mass (Fig. 8(b)) because tire nonlinear restoring forces do not act directly on the body, M_2.

Two types of dominant nonlinearities observed in the restoring force data are considered here: (1) nonlinear shock damping (in the form of both Coulomb friction damping and a deadzone nonlinearity to introduce piecewise-linear damping at higher amplitudes) and (2) hysteretic stiffness (in the form of backlash or mechanical/hydraulic 'play'). Because the restoring force plots in Fig. 4(a)–(d) indicate that the hysteretic stiffness effect dominates in the 0.5–1.0 mm amplitude range whereas the piecewise-linear shock damping effect dominates in the 1.0–7.0 mm range, the system identification procedure is carried out in two steps: first, the hysteretic nonlinearities are identified; and second, the piecewise-linear damping nonlinearities are identified. It was also determined that this two-step approach avoided poor conditioning in the NIFO parameter estimation routine, which does not perform as well when more than one correlated nonlinearity is included in the algorithm simultaneously.

When Coulomb friction is placed in series with a stiffness element, it produces a hysteretic stiffness characteristic that strongly resembles that shown in Fig. 7(b) according to Ferri [16]. Therefore, although Coulomb friction damping is present in the strut as is evident in Fig. 4(a), it is assumed that it can be accounted for in the form of the nonlinear hysteresis and piecewise-linear damping characteristics in the amplitude range from 0.5 to 7.0 mm. This statement is supported by the trends previously described in the subplots in Figs. 3 and 4.

3.3.1. *Backlash nonlinearity*

Consider the hysteretic (backlash) effects in stiffness. Hysteresis in damping was initially considered; however, its effects were small compared to those in stiffness (refer to Fig. 7(a) and (b) for comparison of velocity and displacement ranges over which backlash was observed). The NIFO parameter estimation procedure was carried out as follows for the backlash nonlinearity. First, the backlash restoring force characteristic shown in Fig. 9(a) was generated using a deadband of 0.00043 m based on Fig. 7(b). Note the presence of additional paths back and forth in Fig. 9(a) due to the random response as compared to the single loop seen in Fig. 7(b). It is also observed that the horizontal portions of the hysteresis loops in Fig. 7(b) all occur at the same levels, while those in Fig. 9(a) occur at different horizontal levels. This may indicate that an Iwan-type nonlinearity (series connection of a Coulomb friction element and a linear spring) may be more appropriate, however, it is not pursued here. Second, this describing function was used in the NIFO parameter estimation equations (Eq. (9)) for this single source of nonlinearity given the 1.0 mm input (tire patch displacement) and output (wheel and body acceleration) data. The estimated NIFO functions in this case consist of (1) the estimated true nominal linear transmissibility between the wheel and body, and (2) the nonlinear parameter ratio, $\mu_1(\omega)/K_2$, associated with the backlash describing function in Eq. (8). The nonlinear parameter $\mu_1(\omega)/K_2$ can be thought of as a correction factor, which is applied to the describing function to bring the high- and low-input amplitude data into agreement.

Fig. 9(b) shows plots of the transmissibility magnitudes for three different input levels (0.5, 1.0 and 7.0 mm) for reference as well as the NIFO estimate of the nominal linear transmissibility function $T_{21}(\omega)$. The absence of data below 1.5 Hz is due to the poor low-frequency accuracy obtained using the numerical integrations required to estimate the displacement time histories from the measured acceleration responses. Note that the estimated linear transmissibility function (—) is in good agreement with the 0.5 mm input level transmissibility measurement (⋯). The variations between these two functions could be due either to errors in the backlash describing

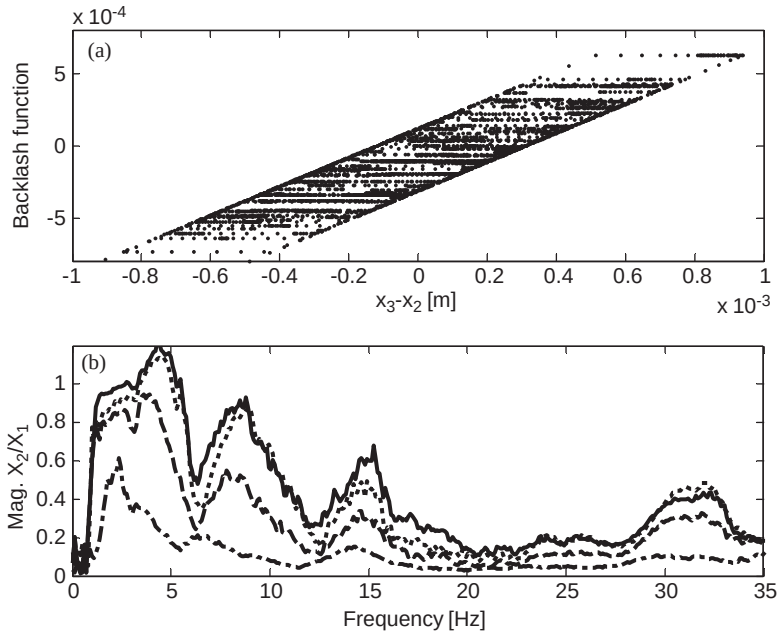

Fig. 9. (a) Backlash describing function between the spindle and body in the strut used in NIFO parameter estimation procedure and (b) magnitudes of measured transmissibility functions between the spindle and body for: ⋯, 0.5 mm; – – –, 1.0 mm; and – · –, 7.0 mm input levels with the NIFO estimate (—) of a near zero level input using the 1.0 mm data.

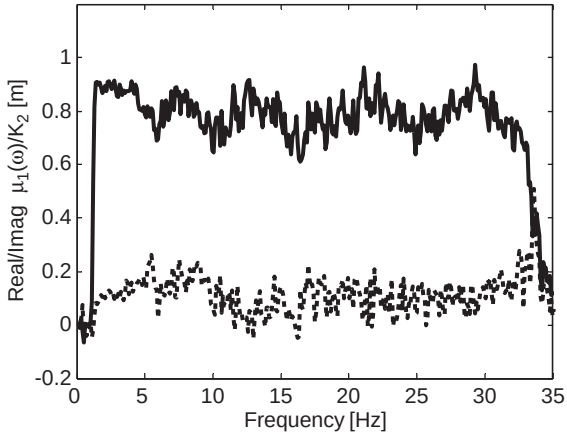

Fig. 10. Real (—) and imaginary (⋯) parts of estimated NIFO parameter, $\mu_1(\omega)/K_2$, for backlash describing function in Fig. 9(a) indicating near zero imaginary part and nearly constant real part as a function of frequency.

function or to additional effects of the backlash nonlinearity if the input level were reduced further from 0.5 mm. The corresponding nonlinear parameter, $\mu_1(\omega)/K_2$, for the backlash nonlinearity is plotted in Fig. 10. The real (—) and imaginary (⋯) parts indicate that $\mu_1(\omega)/K_2$ is

nearly constant as a function of frequency and entirely real. This result implies that the describing function used in Fig. 9(a) is a reasonable choice for this amplitude range.

In order to verify that the tire has negligible effects in this amplitude and frequency range, the nominal linear transmissibility, $H_{11}(\omega)$, between the tire patch and the wheel was estimated as well using the NIFO parameter estimation algorithm with the backlash describing force in Fig. 9(a) and the 1.0 mm input data. The relevant frequency domain parameter estimation equations for NIFO in this case are given in Eq. (10):

$$\begin{bmatrix} X_1(\omega) \\ X_2(\omega) \end{bmatrix} = \begin{bmatrix} H_{11}(\omega)(K_1 + j\omega C_1) & -\mu_1(\omega)(H_{11}(\omega) - H_{12}(\omega)) \\ H_{12}(\omega)(K_1 + j\omega C_1) & -\mu_1(\omega)(H_{21}(\omega) - H_{22}(\omega)) \end{bmatrix} \times \begin{bmatrix} X_b(\omega) \\ X_{n1}(\omega) \end{bmatrix}, \tag{10}$$

where all variables are as defined for Eq. (5) and it is additionally assumed here that the tire behaves relatively linear in this amplitude range with the damping and stiffness coefficients indicated in Fig. 2. Note that $X_{n1}(\omega)$ corresponds to the Fourier transform of the backlash describing function in Fig. 9(a). Also, note that because $H_{22}(\omega)$ cannot be estimated without an input directly applied to the body, NIFO must focus on the first equation in Eq. (10) in order to estimate the nonlinear parameter, $\mu_1(\omega)/(K_1 + j\omega C_1)$, by dividing the second entry of the first row of the parameter matrix by the difference between the entries in the first column.

Fig. 11 shows a plot of the $H_{11}(\omega)$ estimate for a near zero level input compared to the other input level measurements. As in Fig. 9(b), there is good agreement between the zero level $H_{11}(\omega)$ NIFO estimate (—) and the 0.5 mm input level measurement (···) as expected. The only significant errors between these two functions are in the 7–10 Hz range. These three results (Figs. 9(b), 10 and 11) indicate that the dominant nonlinearity in the path between the input and the body in the 0.5–1.0 mm input range is a backlash stiffness nonlinearity (Fig. 9(a)) in the strut. The estimated nonlinear parameter results for $\mu_1(\omega)/(K_1 + j\omega C_1)$ obtained using the input data are not

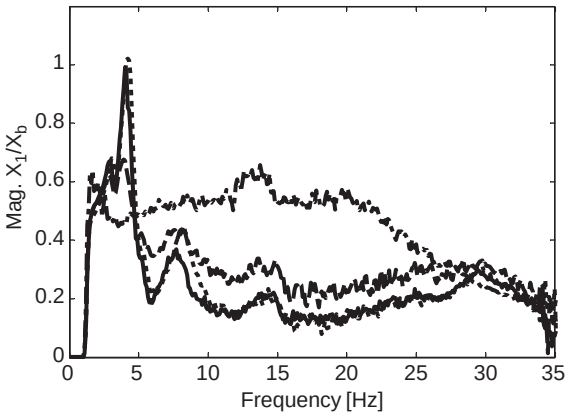

Fig. 11. Magnitudes of measured transmissibility functions between the tire patch and wheel for: ···, 0.5 mm; – – –, 1.0 mm; and – · –, 7.0 mm input levels with the NIFO estimate (—) of a near zero level input using the 1.0 mm data.

discussed here because they require knowledge of the nominal tire stiffness and damping coefficients, which are beyond the scope of this investigation.

3.3.2. Clearance nonlinearity

Next consider the transition from primarily hysteretic damping to a typical piecewise-linear shock damping near 1.0 mm input amplitude (refer to Figs. 4(a) and (b)). It is evident that as the input amplitude is further increased from 1.0 to 7.0 mm, the overall damping restoring force changes from nearly all saturation-type to piecewise-linear in nature. Although there is clearly asymmetry in the piecewise-linear damping characteristic obtained in the restoring force plot in Fig. 4(d), symmetry is assumed here because the use of asymmetrical damping was not observed to produce significantly improved results.

The form of the deadzone describing function used in the subsequent NIFO parameter estimation algorithm in the input amplitude range from 1.0 to 7.0 mm is shown in Fig. 12(a). Recall that this nonlinear form ensures that in addition to the linear damping that is present in the steepest portion of the restoring force loops in Fig. 7(a), an additional and sudden gain in damping in the shock occurs at approximately 0.03 m/s (and symmetrically –0.03 m/s) as the input amplitude is increased. In other words, as the relative velocity across the shock increases, the steep damping characteristic in Fig. 4(a) decreases in a piecewise-linear manner in Figs. 4(b)–(d) due to the additional effects of the nonlinear describing function in Fig. 12(a). The 1.0 mm input amplitude response was taken as the lowest input amplitude level in this application of the NIFO

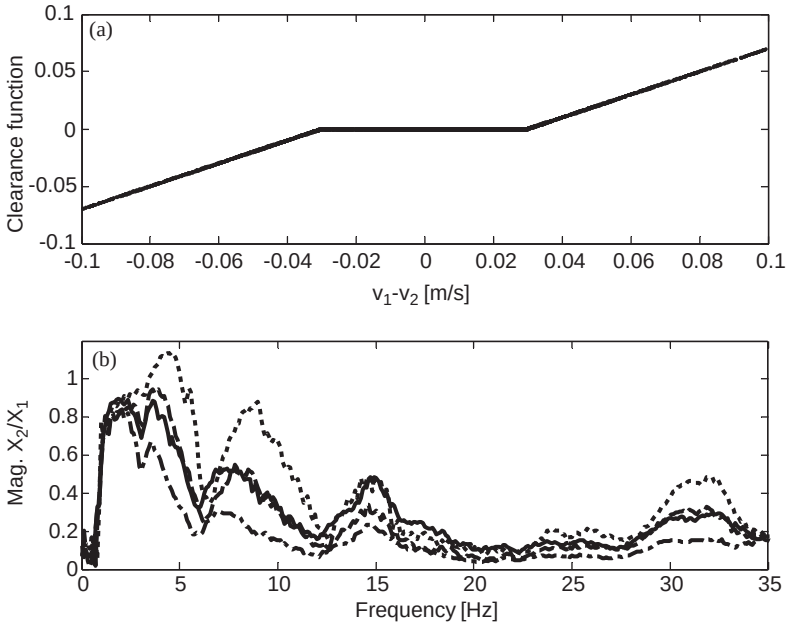

Fig. 12. (a) Clearance (deadzone) describing function between the wheel and body in the strut used in NIFO parameter estimation procedure and (b) magnitudes of measured transmissibility functions between the spindle and body for: ⋯, 0.5 mm; – – –, 1.0 mm; and – · –, 2.5 mm input levels with the NIFO estimate (—) of a near 1.0 mm level input using the 2.5 mm data.

identification technique because the clearance nonlinearity began to emerge just above a 1.0 mm tire patch displacement.

When the nonlinear dead-zone characteristic was used in the NIFO parameter estimation procedure, the wheel and body response data for 5.0 mm (higher operating level) produced the NIFO estimate of $T_{21}(\omega)$ shown in Fig. 12(b) for the 1.0 mm transmissibility function (lower operating level). Note that the NIFO estimate (—) is in good agreement with the 1.0 mm input level transmissibility (– · –) and deviates only slightly in the lower frequency range from 6 to 8 Hz. The NIFO estimate matches particularly well above 20 Hz indicating that nonlinear shock damping dominates in that frequency range.

The estimate of the nonlinear coefficient, $\mu_2(\omega)/K_2$, is shown in Fig. 13. The real (—) and imaginary (···) parts indicate that $\mu_2(\omega)/K_2$ is almost entirely imaginary and varies as a function of frequency. The nonlinear parameter is imaginary because although the nonlinear clearance force is proportional to the relative velocity across the strut, it is in phase with the relative displacement resulting in a 90° phase shift of the describing function's effects in the NIFO parameter estimation algorithm. Also, note that this estimate exhibits frequency dependence in the frequency range of interest. The frequency-dependent nature of the shock damping is expected and was discussed previously in Section 3.2 in the context of the restoring force data in Fig. 5. Moreover, the decrease in $\mu_2(\omega)/K_2$ for increasing frequency supports the trends seen in the restoring force plots from Fig. 5(a)–(d) in which the nonlinear limiting nature of the shock damping becomes less apparent as the frequency in the sine sweep increases. This latter point emphasizes one of the advantages of the proposed approach for nonlinear system identification, that is, the NIFO technique accommodates both nonlinear and frequency-dependent characteristics, which are both found in the majority of mechanical systems.

In order to verify that the tire has negligible effects in this amplitude and frequency range, the nominal linear transmissibility, $H_{11}(\omega)$, between the tire patch and the wheel was estimated as for the backlash nonlinearity in the lower amplitude range. Fig. 14 shows a plot of the $H_{11}(\omega)$ estimate for an input level near 1.0 mm compared to several other input level measurements. As in

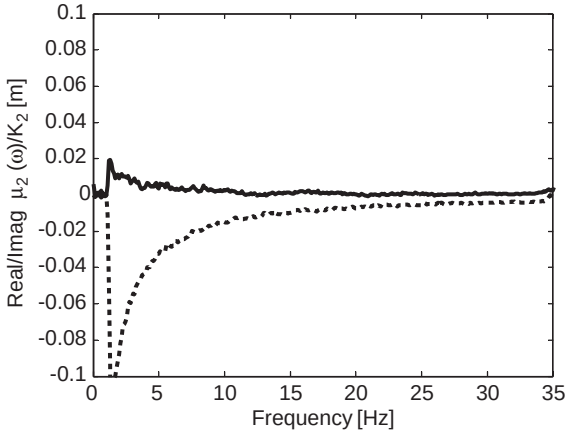

Fig. 13. Real (—) and imaginary (···) parts of estimated NIFO parameter, $\mu_2(\omega)/K_2$, for clearance describing function in Fig. 12(a) indicating near zero real part and nearly constant imaginary part as a function of frequency.

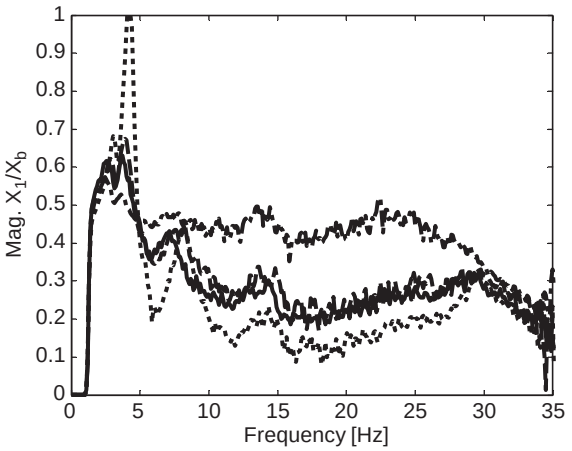

Fig. 14. Magnitudes of measured transmissibility functions between the tire patch and wheel for: ⋯, 0.5 mm; – – –, 1.0 mm; and – · –, 2.5 mm input levels with the NIFO estimate (—) of a near 1.0 mm level input using the 2.5 mm data.

Fig. 12(b), there is good agreement between the 1.0 mm level $H_{11}(\omega)$ NIFO estimate (—) and the 1.0 mm input level measurement (– – –). Thus, the resulting model based on the use of the nominal linear transmissibility function in Fig. 12(b) at 1.0 mm and the nonlinear parameter in Fig. 13 can be used to describe the amplitude and frequency dependencies of the strut in the amplitude range from 1.0 to 2.5 mm. These three results (Figs. 12(b), 13 and 14) indicate that the dominant nonlinearity in the path between the input and the body in the 1.0–2.5 mm input range is a piecewise-linear shock damping nonlinearity (Fig. 12(a)) in the strut. Similar results hold for the higher amplitude ranges as well when tire nonlinearities are included in the analysis.

4. Conclusions

It was demonstrated using vehicle data over given amplitude (0.5–2.5 mm) and frequency (2–30 Hz) ranges that nonlinear mechanical system models can be identified from experimental data using a frequency domain method (NIFO) even in the absence of input data at the tire patch. It was noted that in many mechanical systems, inputs are not readily measured or estimated, including applications where vehicle operating data is taken and post-processed to develop engineering design models. A combination of time domain techniques (restoring force method) and frequency domain system identification algorithms (NIFO) was applied for specific amplitude ranges, from 0.5 to 1.0 mm and 1.0 to 2.5 mm, thereby avoiding ill conditioning in the parameter estimation process, to first characterize and then identify the frequency and amplitude characteristics of the nonlinearities in a test vehicle. Results were verified using the nonlinear model to estimate measured transmissibilities at various amplitudes with and without the hydraulic shaker input at the tire patch.

References

[1] K.S. Mohammed, K. Worden, G.R. Tomlinson, Direct parameter estimation for linear and non-linear structures, *Journal of Sound and Vibration* 152 (3) (1992) 471–499.
[2] C.M. Richards, R. Singh, Identification of multi-degree-of-freedom non-linear systems under random excitations by the "reverse path" spectral method, *Journal of Sound and Vibration* 213 (4) (1998) 673–708.
[3] J.S. Bendat, *Nonlinear Systems Techniques*, Wiley, New York, 1999.
[4] J.B. Roberts, J.F. Dunne, A. Debunos, A spectral method for estimation of non-linear system parameters from measured response, *Probabilistic Engineering Mechanics* 10 (1995) 199–207.
[5] S.F. Masri, T.K. Caughey, R.K. Miller, A.F. Saud, Identification of nonlinear vibrating structures: Part I—formulation, *Journal of Applied Mechanics* 54 (1987) 918–922.
[6] S.F. Masri, T.K. Caughey, R.K. Miller, A.F. Saud, Identification of nonlinear vibrating structures: Part II—applications, *Journal of Applied Mechanics* 54 (1987) 923–929.
[7] K. Yi, K. Hedrick, Observer-based identification of nonlinear system parameters, *Journal of Dynamic Systems, Measurement, and Control* 117 (1995) 175–182.
[8] D.E. Adams, A spatial approach to nonlinear vibration analysis, *Doctoral Dissertation*, University of Cincinnati, 2000.
[9] W.M. Siebert, *Signals and Systems*, McGraw Hill, New York, 1986.
[10] R.N. Bracewell, *The Fourier Transform and its Applications*, second ed., WCB/McGraw-Hill, Boston, 1986.
[11] N. Thrane, *The Hilbert Transform*, Hewlett Packard Application Notes, 1984.
[12] C.K. Chui, *An Introduction to Wavelets*, Academic Press, San Diego, 1992.
[13] D.M. Storer, G.R. Tomlinson, Recent developments in the measurement and interpretation of higher order transfer functions from non-linear structures, *Mechanical Systems and Signal Processing* 7 (2) (1993) 173–189.
[14] S. Cafferty, K. Worden, G. Tomlinson, Characterization of automotive shock absorbers using random excitation, *Journal of Automobile Engineering: Part D* 209 (1995) 239–248.
[15] A.L. Audenino, G. Belingardi, Modeling the dynamic behavior of a motorcycle damper, *Journal of Automobile Engineering: Part D* 209 (1995) 249–262.
[16] A.A. Ferri, Friction damping and isolation systems, *ASME Journal of Vibration and Acoustics* 117B (1995) 196–206.